Climate-induced rebound and exhumation of the European Alps

Charlotte E. Cederbom
Hugh D. Sinclair
CRUST Consortium, School of GeoSciences, University of Edinburgh, Edinburgh EH9 3JW, UK
Fritz Schlunegger Geological Institute, University of Bern, Baltzerstrasse 1, CH-3012 Bern, Switzerland
Meinert K. Rahn Swiss Federal Nuclear Safety Inspectorate, 5232 Villigen-HSK, Switzerland

ABSTRACT

Foreland basins record the regional isostatic compensation of mountain belts; during periods of crustal thickening, they subside, and when erosion unloads the mass of the mountains, the basins rebound and are eroded. In order to evaluate this mechanism for rebound, it is critical that the timing and magnitude of erosion are documented. We present data estimating the timing and magnitude of late orogenic or postorogenic erosion in the North Alpine Foreland Basin of Switzerland. Mineral cooling ages demonstrate that the basin underwent 1–3 km of erosion soon after 5 Ma. This erosion coincided with a decline in structural deformation in the Swiss Alps, and a doubling of sediment accumulation rates in surrounding depocenters. We propose that accelerated erosional unroofing of the Swiss Alps triggered isostatic rebound and erosion of the foreland basin after 5 Ma. A projection of the isostatic rebound of the basin into the mountains suggests that at least 6.5 km of erosion should have occurred in the high topography of the Aar Massif. Accelerated erosion in the Swiss Alps at that time is explained by an increase in atmospheric moisture driven by an intensification of the Atlantic Gulf Stream at 4.6 Ma. Consequently, we propose that the changing erosional capacity of the climate triggered late orogenic to postorogenic mass reduction and isostatic rebound of the Swiss Alps and their neighboring foreland basin.

Keywords: climate effects, exhumation, fission tracks, foreland basins, mountains, erosion.

INTRODUCTION

The North Alpine Foreland Basin provides a depositional record of the early Oligocene to early or middle Miocene tectonic evolution in the northern part of the European Alps. A major unconformity between lower or middle Miocene and Quaternary sedimentary rocks precludes any direct information on the northern Alps and their foreland since ca. 12 Ma. Vitrinite-reflectance, stratigraphic, and clay-mineral transformation analyses and seismic velocity anomaly studies in the North Alpine Foreland Basin suggest that the sub-Quaternary unconformity is a result of ~2 km of erosion in the southwest (Geneva), diminishing to ~0.3 km in the northeast (Zürich), while middle to late Miocene paleo–geothermal gradients of 15–30 °C/km prevailed (Laubscher, 1974; Lemcke, 1974; Monnier, 1982; Schaer, 1992; Schegg, 1992, 1994; Schegg and Leu, 1998). Late Miocene–Pliocene northward thrusting of the basin succession led to tectonic shortening in the Jura fold-and-thrust belt farther north, which previously has been regarded as the main mechanism for late Cenozoic erosion in the foreland basin (Laubscher, 1974; Pfiffner et al., 1997; Burkhard and Sommaruga, 1998).

Here we use a novel approach to estimate the timing and amount of late orogenic to postorogenic erosion in the North Alpine Foreland Basin. The results suggest an alternative driving mechanism for the recorded late Cenozoic exhumation in both the foreland basin and the Swiss Alps.

METHOD

We present apatite fission-track (FT) data from three vertical profiles (Boswil, Hünenberg, and Rigi-Weggis) along a transect across the North Alpine Foreland Basin, including the ''undeformed'' Plateau Molasse in the north and the thrust-faulted Subalpine Molasse adjacent to the mountain belt in the south (Fig. 1). The apatite FT thermochronometer has a closure temperature of ~120 °C, but the fission tracks begin being partially annealed at ~60 °C, and a reduction of both track length and FT age takes place in the partial annealing zone (PAZ) between ~60 and 120 °C (Gleadow and Duddy, 1982). In sedimentary basins a typical apatite FT age versus depth trend (Fig. 2) comprises old detrital FT ages (older than or equal to the depositional age) above the PAZ, continuously decreasing FT ages within the PAZ, and zero FT ages below the PAZ. The upper part of the PAZ may even include FT ages that are older and constant with depth if the detrital FT ages increase with depth. Rapid erosion of the basin causes an upward shift of this age versus depth distribution, which enables an estimate of the timing and amount of erosion. The depth to the top of the PAZ (y) and its interval thickness (a) prior to exhumation (Fig. 2) are dependent on the paleo–geothermal gradient immediately before and at the time of exhumation (t). The present FT age distribution down a vertical profile provides information about the present-day depth to the top ($y - x$) and/or bottom

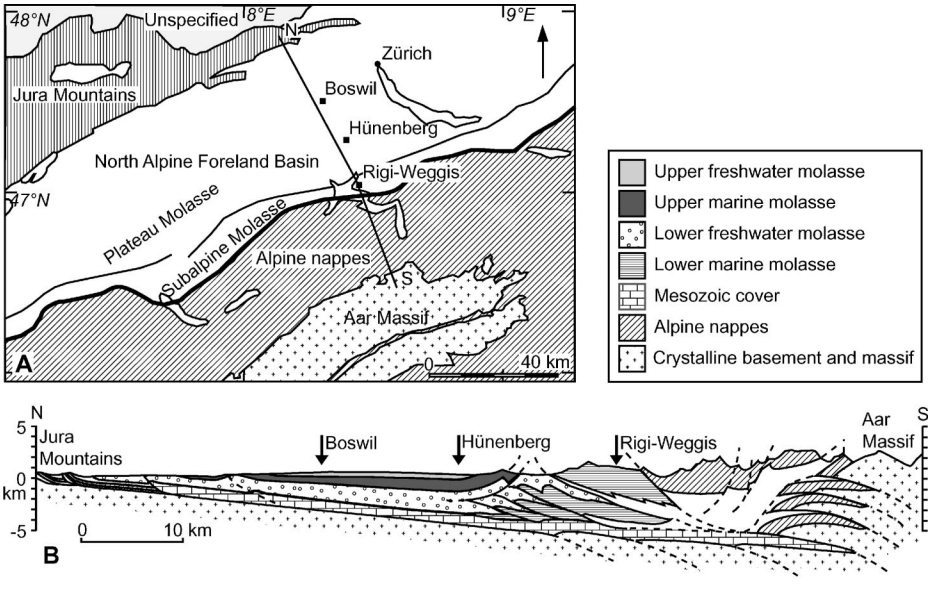

Figure 1. A: Tectonic map of Swiss part of North Alpine Foreland Basin and Alps, with location of three boreholes and extent of cross section illustrated in B. Bold curve marks Alpine thrust front. B: Cross section through Swiss part of North Alpine Foreland Basin and Alps (modified from Burkhard, 1990). Arrows mark projected positions of vertical sections.

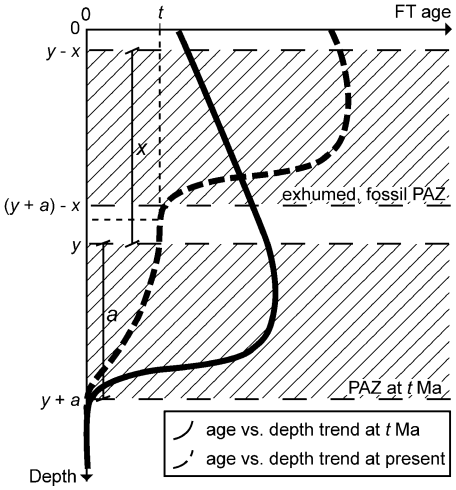

Figure 2. Schematic illustration of apatite fission-track (FT) age trends with depth at time of exhumation (*t*) and at present day. For simplification of figure, it is assumed that width of present-day partial annealing zone (PAZ) is equal to width of fossil PAZ (*a*), i.e., that geothermal gradient has not changed since time *t*. See text for explanation of calculation of amount of erosion (*x*).

$[(y + a) - x]$ of the fossil PAZ, from which the amount of erosion (x) can be calculated. The deepest FT sample in the section, from above the present-day PAZ, provides a maximum value of t if the sample is partially annealed and is located within the fossil PAZ. Alternatively, if the sample belongs to a fossil zone of total annealing (Fig. 2; i.e., the FT clock has been reset to zero), it provides a minimum or exact value of t, depending on the erosion rate.

RESULTS

The three vertical sampling profiles are all situated above or in the uppermost part of the present-day PAZ (Fig. 3). The spread among the single-grain FT ages for each sample is large, but the age interval over which they span decreases toward the bottom. In addition, the proportion of single-grain FT ages that are younger than the depositional age increases (Fig. 3; see also Table DR1[1]). These observations illustrate partial annealing, above the present-day PAZ, that increases in strength with depth in all three sections. The pooled FT age pattern illustrates an age versus depth trend that is typical for a PAZ, and because it is located above the present-day PAZ, it represents a fossil PAZ. For the deepest sample in the Boswil section, the detrital signature is still strong, and the pooled FT age thus lacks temporal significance. Nevertheless, this sample includes several young single-grain FT ages, and generates a peak in the probability density curve at 5.3 Ma (Fig. 3), which can be regarded as a maximum age for the cooling of this section. The deepest sample in the Hünenberg profile indicates total annealing, but was collected within the present-day PAZ. The pooled FT age of 3.6 ± 1.0 Ma (±2σ) is thus regarded as a minimum age for the cooling. The second deepest sample is only partially annealed, but provides a maximum age in the form of a peak in the probability curve at 5.5 Ma. The lower part of the Rigi-Weggis profile is thrust faulted, but provides pooled FT ages for the strongly annealed deepest and third-deepest samples of 4.7 ± 1.0 and 4.8 ± 2.2 Ma, respectively. Additionally, the peak in the probability curve for the second-deepest, but less annealed, sample is at 4.8 Ma, implying cooling later than ca. 4.8 Ma.

The recorded early Pliocene cooling may have been caused by a reduction in geother-

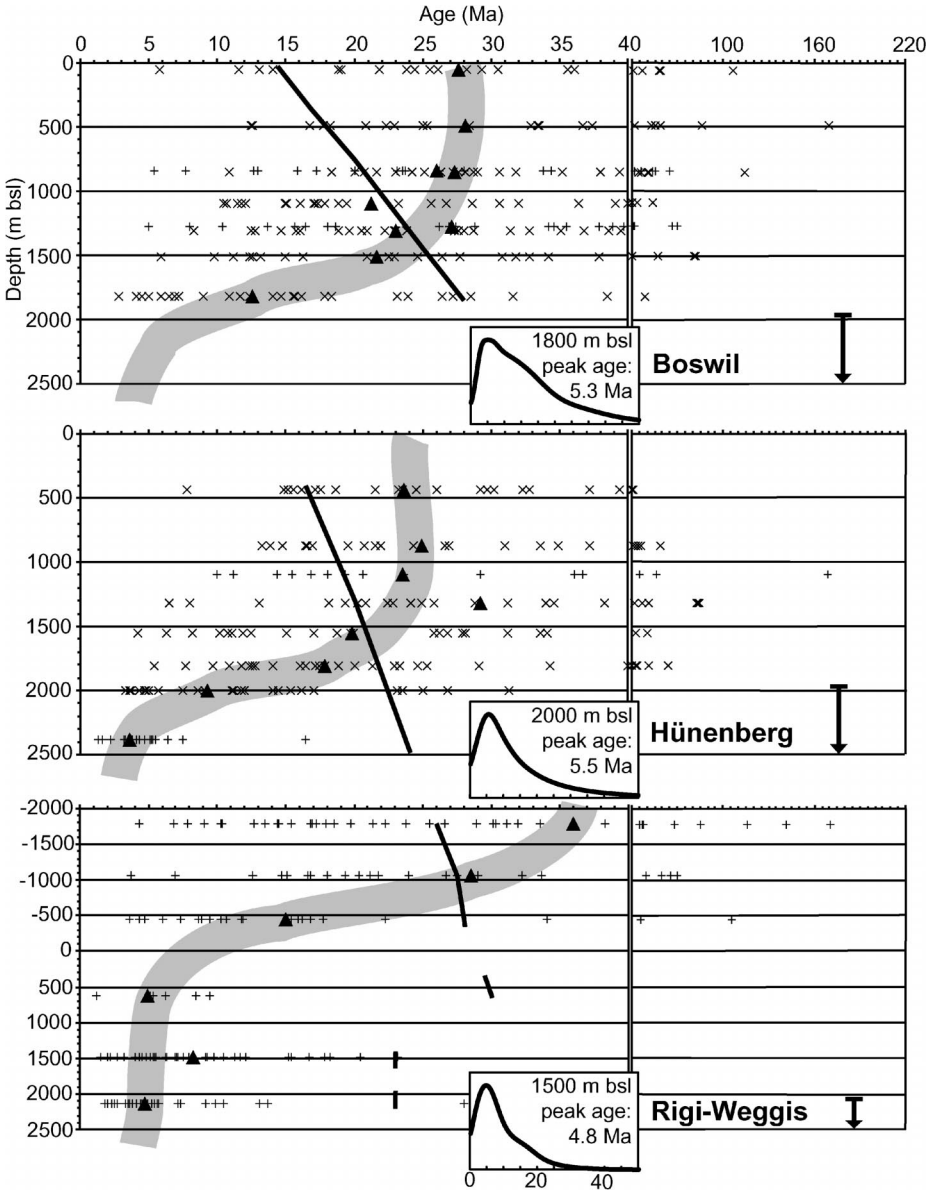

Figure 3. Fission-track (FT) results from three vertical sections in North Alpine Foreland Basin; single-grain FT ages (x and plus symbols; analysts, Cederbom and Rahn, respectively) and pooled FT ages (black triangles). Thin black line represents depositional age trend in each borehole. Arrow marks position of present-day partial annealing zone. Note that *x*-axes vary in scale along axis, and that Rigi-Weggis section includes both outcrop and borehole samples. Inset figures show probability density curves for deepest (Boswil) and second-deepest (Hünenberg and Rigi-Weggis) samples, respectively. Single-grain age scatter illustrates influence of detrital signature. For partially annealed samples, pooled FT ages lack temporal significance but illustrate trend of decreasing FT age with depth below sea level (bsl). (For detailed compilation of analytical procedure, precision of single-grain ages, central FT ages, probability density curves, kinetic variability for each sample, and explanation of pooled vs. central FT age, see Appendix DR1 [text footnote 1].)

[1]GSA Data Repository item 2004116, Appendix DR1, Table DR1, and Figure DR1, is available online at www.geosociety.org/pubs/ft2004.htm, or on request from editing@geosociety.org or Documents Secretary, GSA, P.O. Box 9140, Boulder, CO 80301-9140, USA.

TABLE 1. CALCULATION OF MINIMUM AND MAXIMUM VALUES OF THE EROSION ESTIMATE IN THE NORTH ALPINE FORELAND BASIN AND ISOSTATIC COMPONENT IN THE AAR MASSIF

	Paleo–geothermal gradient (°C/km)	y^* (km)	a^* (km)	$y - x^*$ (km)	$(y + a) - x^*$ (km)	x^* (km)	Erosion estimate (km)	Structural component (km)	Isostatic component (km)	Predicted vertical displacement (%)	Isostatic component in the Aar Massif (km)
Boswil							1.7–3.5	0.4	1.3–3.1	17–20	6.5–18.2
minimum	30	1.7	2	**0**	2	1.7					
maximum	20	2.5	3	−1	**2**	3.5					
Hünenberg							1.4–3.3	0.4	1.0–2.9	29–32	3.1–10.0
minimum	30	1.7	2	**0.3**	2.3	1.4					
maximum	20	2.5	3	−1.2	**2.2**	3.3					
Rigi-Weggis							3.8–6.1	0.4	3.4–5.7	45–47	7.2–12.7
minimum	25	2	2.4	−0.3	**2.1**	(2.3)					
minimum	25	2	2.4	−**1.8**	0.6	3.8					
maximum	15	2.7	4	−3.4	**0.6**	6.1					
Aar Massif										100	

Note: Bold numbers are numbers obtained from Figure 3; the number in parentheses is not reasonable on the basis of the FT results; therefore, an alternative minimum estimate has been calculated; structural component is the maximum erosion generated by shortening in the Jura Mountains; isostatic component = erosion estimate – structural component; the predicted vertical displacement is based on minimum and maximum values for the flexural rigidity and is a percentage of the displacement in the Aar Massif; the isostatic component in the Aar Massif is calculated by using the predicted displacement and the isostatic component for each profile.
*See Figure 2.

mal gradient, erosional unroofing, or a combination of these two. Minimum and maximum erosion estimates for each profile are presented in Table 1. They have been calculated by using minimum values for the depth to the top or bottom of the fossil PAZ and the range of probable paleo–geothermal gradients for each well. The provenance regions for the sediments in the North Alpine Foreland Basin have been identified (Schlunegger et al., 1997), revealing that the detrital FT ages probably increased significantly with depth and that they are considerably older than the corresponding depositional age. This finding suggests that the FT ages should increase, and/or remain constant, with depth in the upper part of the fossil PAZ. The geothermal gradient during latest Miocene and Pliocene time is unlikely to have exceeded 30 °C/km and was decreasing toward the south (Schegg and Leu, 1998; Rahn and Grasemann, 1999). Previously published estimates of the paleo–geothermal gradient and the erosion from the Weggis borehole are 20–23 °C/km and 4.1 km, respectively, based on vitrinite-reflectance data (Schegg, 1994). At present, low gradients are recorded in the boreholes: 30 °C/km for 0–1 km below sea level and 22–23 °C/km below 1 km depth in Boswil and Hünenberg and ~22 °C/km in the Weggis borehole. Using a paleo–geothermal gradient similar to that of today (23 °C/km), these calculations imply erosion values of 2.2–2.8 km and 1.9–2.6 km for Boswil and Hünenberg, respectively, and 4.2–4.5 km (22 °C/km) for Rigi-Weggis. Together, the three vertical profiles reveal that the sub-Quaternary unconformity in the North Alpine Foreland Basin records extensive erosion during early Pliocene time.

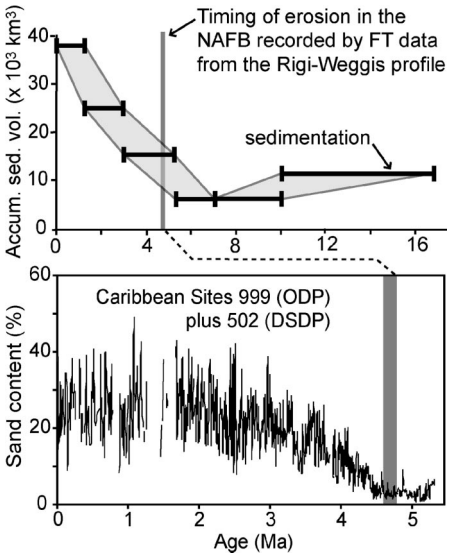

Figure 4. Total accumulated sediment volumes in adjacent depositional settings (Rhône Delta, Rhône Graben plus molasse, and North Sea [Kuhlemann, 2000]) and percentage of sand in Caribbean sediments (Prell, 1982; Haug and Tiedemann, 1998). Plots illustrate temporal coincidence of acceleration in sediment discharge from Swiss and Western Alps, closure of Isthmus of Panama (which led to increase in atmospheric moisture over Eurasia), and maximum timing of erosion recorded by fission-track (FT) data in North Alpine Foreland Basin (NAFB). ODP—Ocean Drilling Program; DSDP—Deep Sea Drilling Project.

DRIVING MECHANISM

The Pliocene shortening across the easternmost part of the Jura Mountains was <5 km (Burkhard, 1990) and was executed along thrust planes dipping <5° (Pfiffner et al., 1997). The maximum amount of rock uplift and potential erosion in the North Alpine Foreland Basin generated by this shortening is 0.44 km, a value far lower than our minimum estimates for the three sections. Consequently, an additional mechanism must have been present. Rates of crustal thickening in the Swiss Alps were declining or halted during Pliocene time (Schmid et al., 1996). Nevertheless, there was at least a doubling of erosion rates in the Swiss and Western Alps ca. 5–4 Ma (Kuhlemann et al., 2001), as shown by the sedimentation records in surrounding depositional settings (Fig. 4; Kuhlemann, 2000). It is therefore probable that the erosional unroofing of the Alps was greater than the crustal thickening, which implies a net reduction in the total mass of the mountain belt. A mass reduction would have been regionally compensated by flexural uplift of the underlying plates, and hence caused flexural rebound and erosion of the foreland basin (e.g., Watts, 2001). This mechanism provides an explanation for the large component of erosion of the North Alpine Foreland Basin succession that cannot be explained by shortening in the Jura. Another possibility is that a major drop in base level linked to the Messinian salinity crisis (Krijgsman et al., 1999) may have driven incision of rivers throughout southern Europe. However, the only possible major river that could have induced significant erosion is the Rhône, and it has been demonstrated that the Messinian knickpoint of the Rhône never reached the North Alpine Foreland Basin (Clauzon and Rubino, 1995). Alternative mechanisms to drive isostatic rebound of the North Alpine Foreland Basin would involve mantle dynamics in response to slab detachment (Lyon-Caen and Molnar, 1989) or a retarded response to overthickening of the Alps (Holliger and Kissling, 1992), but neither of them is constrained in time or supported by geological observations. In contrast, we have knowledge of the climatic history of the region that enables a further exploration of the enhanced Alpine unroofing and isostatic rebound hypothesis.

The climate of western Europe is dominated by the Atlantic Gulf Stream, and an intensification of the Gulf Stream, as it exists today, was determined by the closure of the Isthmus of Panama at 4.6 Ma (Fig. 4; Haug and Tiedemann, 1998). It has been proposed that this

intensification of the Gulf Stream resulted in increased atmospheric moisture and stream runoff from the rivers of Eurasia (Driscoll and Haug, 1998). We further propose that the increase in atmospheric moisture brought in by the Gulf Stream and the accelerated erosion around the Alps (Fig. 4) are physically related. In this scenario, isostatic rebound of the North Alpine Foreland Basin was initiated by an acceleration of erosional unroofing in the Alps driven by increased precipitation after 4.6 Ma.

If the rebound of the foreland basin was driven by enhanced erosional removal of mass in the mountain belt, then, using the approximation of a broken elastic plate, we can broadly predict the amount of erosion of the mountain belt required to drive the documented rebound of the basin. For the calculations, we use the range 1.3–3.1 km for isostatic rock uplift at Boswil (isostatic component; Table 1) and an effective elastic thickness of 20 ± 5 km for the lithosphere underlying the North Alpine Foreland Basin along this traverse (Stewart and Watts, 1997). Flexural theory predicts that the time-equivalent rock uplift at a point 70 km south into the mountain belt (the drainage divide of the Aar Massif) would be five times the value for the foreland basin, yielding a minimum of 6.5 km (Table 1). Numerous apatite FT ages younger than 5 Ma clustered in the region of the Aar Massif complement this prediction (Michalski and Soom, 1990; Lihou et al., 1995). However, the signature of young thermochronometric ages is not uniform and points to a complex distribution of erosion in the mountain belt. This might be expected for a region that has undergone a complex regional distribution of erosion during multiple glacial and interglacial cycles, accompanied by highly localized orographic enhancement of precipitation (Frei and Schaer, 1999).

CONCLUDING REMARKS

We conclude that the sub-Quaternary unconformity in the Swiss part of the North Alpine Foreland Basin records extensive erosion during early Pliocene time. Apart from the component of erosion associated with tectonic shortening in the basin, at least ~1–3 km of the unroofing along the transect was driven by an additional mechanism. The most probable explanation for this post–5 Ma erosional unroofing of the North Alpine Foreland Basin is the isostatic rebound of the mountain belt in response to a wetter climate, induced by the intensification of the Gulf Stream in the Atlantic at 4.6 Ma. The interpretation is difficult to reconcile with the view that a component of the Alps has been in exhumational steady state from 18 Ma to present (Bernet et al., 2001).

ACKNOWLEDGMENTS

We thank W. Leu for well data and practical support, P. Lahusen (SEAG [Schweizerische Erdöl AB]) for the sampling permission and SEAG AG for providing the samples, the National Cooperative for the Disposal of Radioactive Waste for access to well data, G. Haug for supplying Caribbean data, and P. van der Beek, T. Dempster, and C. Persano for discussions. S. Schmid and G. Haug are acknowledged for constructive reviews. The project was financed by the Scottish Higher Education Funding Council.

REFERENCES CITED

Bernet, M., Zattin, M., Garver, J.I., Brandon, M., and Vance, J.A., 2001, Steady-state exhumation of the European Alps: Geology, v. 29, p. 35–38.

Burkhard, M., 1990, Aspects of the large-scale Miocene deformation in the most external part of the Swiss Alps (Subalpine Molasse to Jura fold belt): Eclogae Geologicae Helvetiae, v. 83, p. 559–583.

Burkhard, M., and Sommaruga, A., 1998, Evolution of the western Swiss Molasse basin: Structural relations with the Alps and the Jura belt, *in* Mascle, A., et al., eds., Cenozoic foreland basins of western Europe: Geological Society [London] Special Publication 143, p. 279–298.

Clauzon, G., and Rubino, J.-L., 1995, Peri-Mediterranean Pliocene basins are very large scale incised valleys filled by Gilbert-type fan deltas: American Association of Petroleum Geologists Bulletin, v. 79, p. 1203–1204.

Driscoll, N., and Haug, G.H., 1998, A short-circuit in thermohaline circulation: A cause for Northern Hemisphere glaciation?: Science, v. 282, p. 436–438.

Frei, C., and Schaer, C., 1999, A precipitation climatology of the Alps from high resolution rain gauge observations: Journal of Climatology, v. 18, p. 873–900.

Gleadow, A.J.W., and Duddy, I.R., 1982, A natural long-term track annealing experiment for apatite: Nuclear Tracks, v. 5, p. 169–174.

Haug, G.H., and Tiedemann, R., 1998, Effect of the formation of the Isthmus of Panama on Atlantic Ocean thermohaline circulation: Nature, v. 393, p. 673–676.

Holliger, K., and Kissling, E., 1992, Gravity interpretation of a unified 2D acoustic image of the central Alpine collision zone: Geophysical Journal International, v. 111, p. 213–225.

Krijgsman, W., Hilgen, F.J., Raffi, I., Sierro, F.J., and Wilson, D.S., 1999, Chronology, causes and progression of the Messinian salinity crisis: Nature, v. 400, p. 652–655.

Kuhlemann, A., 2000, Post-collisional sediment budget of circum-Alpine basins (central Europe): Padova, Estratto da Memorie di Scienze Geologiche, v. 52, p. 1–91.

Kuhlemann, J., Frisch, W., Dunkl, I., and Székely, B., 2001, Quantifying tectonic versus erosive denudation by the sediment budget: The Miocene core complexes of the Alps: Tectonophysics, v. 330, p. 1–23.

Laubscher, H.P., 1974, Basement uplift and decollement in the Molasse Basin: Eclogae Geologicae Helvetiae, v. 67, p. 531–537.

Lemcke, K., 1974, Vertikalbewegungen des vormesozoischen Sockels im nördlichen Alpenvorland vom Perm bis zur Gegenwart: Eclogae Geologicae Helvetiae, v. 67, p. 121–133.

Lihou, J., Hurford, A., and Carter, A., 1995, Preliminary fission-track ages on zircons and apatites from the Sardona unit, Glarus Alps, eastern Switzerland: Late Miocene–Pliocene exhumation rates: Schweizerische Mineralogische und Petrographische Mitteilungen, v. 75, p. 177–186.

Lyon-Caen, H., and Molnar, P., 1989, Constraints on the deep structure and dynamic processes beneath the Alps and adjacent regions from an analysis of gravity anomalies: Geophysical Journal International, v. 89, p. 19–32.

Michalski, I., and Soom, M., 1990, The Alpine thermotectonic evolution of the Aar and Gotthard massifs, central Switzerland: Fission track ages on zircon and apatite and K-Ar mica ages: Schweizerische Mineralogische und Petrographische Mitteilungen, v. 70, p. 373–387.

Monnier, F., 1982, Thermal diagenesis in the Swiss molasse basin: Implications for oil generation: Canadian Journal of Earth Sciences, v. 19, p. 328–342.

Pfiffner, O.A., Erard, P.-F., and Stäuble, M., 1997, Two cross-sections through the Swiss Molasse Basin (lines E4–E6, W1, W7–W10), *in* Pfiffner, O.A., et al., eds., Deep structure of the Swiss Alps: Results of NRP 20: Basel, Birkhäuser Verlag, p. 64–72.

Prell, W.L., 1982, Oxygen and carbon isotope stratigraphy for the Quaternary of Hole 502B: Evidence for two modes of isotope variability, *in* Prell, W.L., et al., Initial reports of the Deep Sea Drilling Project, Volume 68: Washington, D.C., U.S. Government Printing Office, p. 453–464.

Rahn, M.K., and Grasemann, B., 1999, Fission track and numerical thermal modeling of differential exhumation of the Glarus thrust plane (Switzerland): Earth and Planetary Science Letters, v. 169, p. 245–259.

Schaer, J.-P., 1992, Tectonic evolution and vertical movement in western Switzerland: Eclogae Geologicae Helvetiae, v. 85, p. 695–699.

Schegg, R., 1992, Thermal maturity of the Swiss Molasse Basin: Indications for paleogeothermal anomalies?: Eclogae Geologicae Helvetiae, v. 85, p. 745–764.

Schegg, R., 1994, The coalification profile of the well Weggis (Subalpine Molasse, Central Switzerland): Implications for erosion estimates and the paleogeothermal regime in the external part of the Alps: Swiss Association of Petroleum Geologists and Engineers Bulletin, v. 61, p. 57–67.

Schegg, R., and Leu, W., 1998, Analysis of erosion events and paleogeothermal gradients in the North Alpine Foreland Basin of Switzerland, *in* Duppenbecker, S., and Illife, J.E., eds., Basin modelling: Practice and progress: Geological Society [London] Special Publication 141, p. 137–155.

Schlunegger, F., Jordan, T.E., and Klaper, E.M., 1997, Controls of erosional denudation in the orogen on foreland basin evolution: The Oligocene central Swiss Molasse Basin as an example: Tectonics, v. 16, p. 823–840.

Schmid, S.M., Pfiffner, O.A., Froitzheim, N., Schönborn, G., and Kissling, E., 1996, Geophysical-geological transect and tectonic evolution of the Swiss-Italian Alps: Tectonics, v. 15, p. 1036–1064.

Stewart, J., and Watts, A.B., 1997, Gravity anomalies and spatial variations of flexural rigidity at mountain ranges: Journal of Geophysical Research, v. 102, p. 5327–5352.

Watts, A.B., 2001, Isostasy and flexure of the lithosphere: Cambridge, Cambridge University Press, 458 p.

Manuscript received 23 January 2004
Revised manuscript received 16 April 2004
Manuscript accepted 19 April 2004

Printed in USA